

Scanning triboelectric nanogenerator as a nanoscale probe for measuring local surface charge density on a dielectric film F

Cite as: Appl. Phys. Lett. **118**, 193901 (2021); <https://doi.org/10.1063/5.0051522>
 Submitted: 25 March 2021 . Accepted: 30 April 2021 . Published Online: 10 May 2021

Shiquan Lin, and  Zhong Lin Wang

COLLECTIONS

 This paper was selected as Featured



View Online



Export Citation

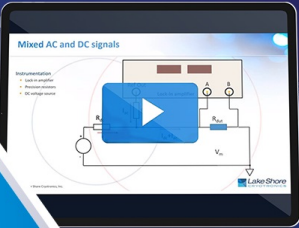


CrossMark



David Daughton, PhD
Applications Scientist
Lake Shore Cryotronics





WEBINAR
A New Concept in Semiconductor
Material/Device Characterization
Combining DC and AC Sourcing and Measuring

Watch Now

Houston Fortney
Development Engineer
Lake Shore Cryotronics





Scanning triboelectric nanogenerator as a nanoscale probe for measuring local surface charge density on a dielectric film

Cite as: Appl. Phys. Lett. **118**, 193901 (2021); doi: [10.1063/5.0051522](https://doi.org/10.1063/5.0051522)

Submitted: 25 March 2021 · Accepted: 30 April 2021 ·

Published Online: 10 May 2021



View Online



Export Citation



CrossMark

Shiquan Lin^{1,2} and Zhong Lin Wang^{1,3,a)} 

AFFILIATIONS

¹Beijing Institute of Nanoenergy and Nanosystems, Chinese Academy of Sciences, Beijing 100083, People's Republic of China

²School of Nanoscience and Technology, University of Chinese Academy of Sciences, Beijing 100049, People's Republic of China

³School of Materials Science and Engineering, Georgia Institute of Technology, Atlanta, Georgia 30332-0245, USA

^{a)} Author to whom correspondence should be addressed: zlwang@binn.cas.cn

ABSTRACT

Inspired by the contact-separation mode triboelectric nanogenerator (TENG), we propose a technique for local surface charge density measurement based on atomic force microscopy. It is named as scanning TENG, in which a conductive tip tapping above a charged dielectric surface produces an AC between the tip and the dielectric bottom electrode due to electrostatic induction. The Fourier analysis shows that the amplitude of the first harmonic of the AC is linearly related to surface charge density. The results demonstrate that the scanning TENG is a powerful tool for probing nanoscale charge transfer in contact-electrification.

Published under an exclusive license by AIP Publishing. <https://doi.org/10.1063/5.0051522>

Since the invention of atomic force microscopy (AFM) in 1986, it has become a powerful tool to look into local material properties at nanoscale. Many different modes and applications based on AFM have emerged with unprecedented impacts, such as conductive atomic force microscopy (CAFM),¹ piezoelectric force microscopy (PFM),² Kelvin probe force microscopy (KPFM),³ electrostatic force microscopy (EFM),⁴ lateral force microscopy (LFM),⁵ magnetic force microscopy (MFM),⁶ and quantitative nanomechanical mapping (QNM).⁷ Recently, local surface charge density measurement method is highly desired owing to the invention of the triboelectric nanogenerator (TENG),^{8–11} since that the charge density on the dielectric surfaces is of great importance for TENG. KPFM is currently the preferred mode for measuring local surface charge density. However, an alternating bias (AC bias) is required to generate electrostatic force on the conductive tip and induce the tip vibration in KPFM mode.¹² It is hard to ensure that the applied AC bias does not affect the accuracy of surface charge density measurement. On the other hand, the output signal in KPFM mode is the applied voltage bias (DC bias), which compensates the potential difference between the conductive tip and sample surface. The relationship between the potential difference and the surface charge density is not intuitively obvious. Therefore, it is necessary to develop a scanning probe microscopy technique for local surface charge density measurement.

Contact-separation mode TENG is one of the most common types of TENGs,^{13,14} which usually consist of a conductive electrode and a dielectric layer with a conductive bottom electrode. When the conductive electrode contacts the dielectric layer, static charges will be generated on the dielectric surface due to the contact-electrification. If the conductive electrode further vibrates near the charged dielectric surface, an AC displacement current will be induced due to electrostatic induction.

Inspired by the contact-separation mode TENG, we designed a mode for local surface charge density measurement based on AFM, which is named as scanning TENG mode. As shown in Fig. 1(a), it can be considered as a nanoscale contact-separation mode TENG when a conductive tip tapping above a dielectric surface with a bottom electrode. If the dielectric surface is charged, an AC between the conductive tip and the bottom electrode will be induced by electrostatic interaction, just like that occurs in the normal size contact-separation TENGs. The amplitude of the AC depends on the density of surface charges, so, in turn, the mapping of the AC amplitude reflects the surface charge distribution. Here, the tip-sample system is approximated as a parallel plated capacitor for simplicity, which is valid especially with considering the gap distance between the tip and the sample is rather small. Figure 1(b) shows the capacitance model for the nanoscale contact-separation mode TENG (scanning TENG), in which the

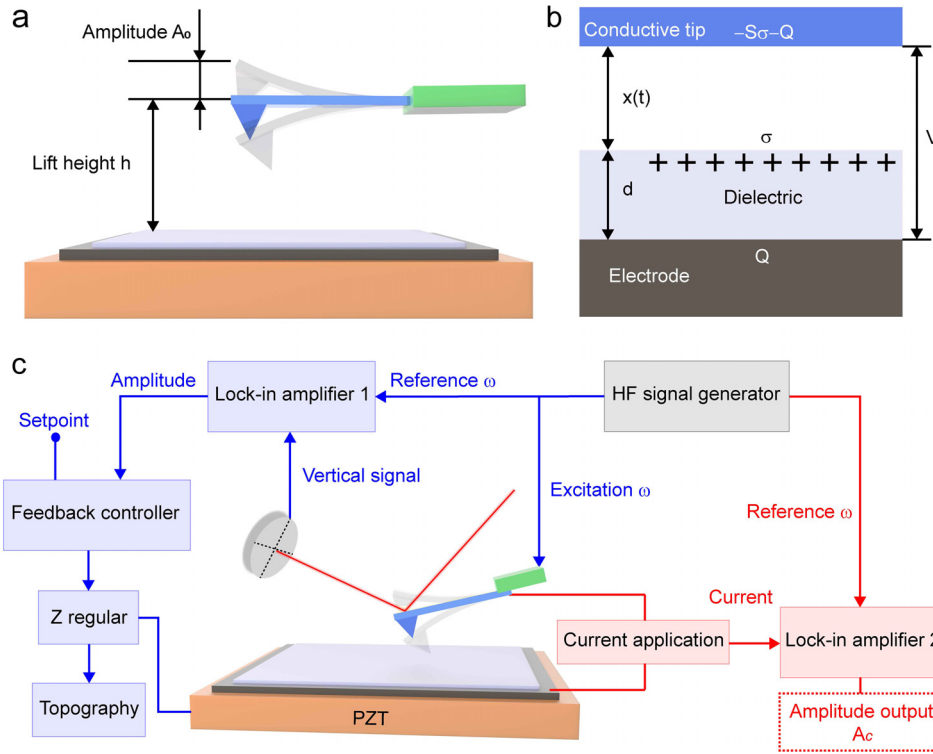


FIG. 1. The setup of the scanning triboelectric nanogenerator (scanning TENG). (a) A conductive tip tapping above a dielectric surface with lift height h and tapping amplitude A_0 , which can be considered as a nanoscale contact-separation TENG or scanning TENG. (b) The capacitance model for scanning TENG. (c) Block diagram of scanning TENG mode.

distance between the tip surface and the dielectric surface can be expressed by the following equation:

$$x(t) = h + A_0 \sin(\omega t), \quad (1)$$

where h denotes the tip lift height, A_0 denotes the tip tapping amplitude [Fig. 1(a)], ω is the tapping frequency of the tip, and t is the time.

We assume that the charge density on the dielectric surface is σ , and the induced charges on the bottom electrode surface (the area covered by the tip) and conductive tip surface are Q and $-S\sigma - Q$ (where S denotes the effective surface area of the tip), respectively. According to the capacitance model, there is a relationship among three parameters:¹⁵ the potential difference between the tip and the bottom electrode (V), the amount of transferred charges in between (Q), and the separation distance between the tip and the dielectric surface [$x(t)$], as shown below:

$$V = -\frac{Q}{S\epsilon_0} \left(\frac{d}{\epsilon} + x(t) \right) - \frac{\sigma x(t)}{\epsilon_0}, \quad (2)$$

where d denotes the thickness of the dielectric film, ϵ_0 is the vacuum dielectric constant, and ϵ is the relative dielectric constant of the dielectric film.

Combining Eq. (1), Eq. (2) can also be expressed as follows:

$$Q(t) = \frac{S(-\sigma(h + A_0 \sin(\omega t)) - \epsilon_0 V)}{\frac{d}{\epsilon} + h + A_0 \sin(\omega t)}. \quad (3)$$

By taking the derivative of Eq. (3), we can obtain an expression for the current between the tip and the bottom electrode during tapping as follows:

$$I(t) = Q'(t) = \frac{S \left(\epsilon_0 V - \frac{\sigma d}{\epsilon} \right) A_0 \omega \cos(\omega t)}{\left(\frac{d}{\epsilon} + h + A_0 \sin(\omega t) \right)^2}. \quad (4)$$

Equation (4) suggests that the AC between the tip and the bottom electrode has different frequency components. Here, we focus on the first harmonic of the AC, which is extracted as follows, and the details of the derivations are shown in [supplementary material](#) note 1,

$$I(t)_\omega = \left(\frac{d + \epsilon h}{\sqrt{(d + \epsilon h)^2 - (\epsilon A_0)^2}} - 1 \right) \frac{2\omega S(\epsilon \epsilon_0 V - \sigma d)}{\epsilon A_0} \cos(\omega t). \quad (5)$$

In Eq. (5), the amplitude of the first harmonic of the current is linearly related to the surface charge density (σ), which implies that if all other parameters in Eq. (5) are known and the amplitude of the first harmonic of the current is measured, the charge density on the dielectric surface can be obtained.

Figure 1(c) gives the block diagram of the scanning TENG, in which the amplitude of the first harmonic of the induced current is to be measured. In the scanning TENG mode, the two-pass technique is used.¹² The blue block diagrams show the first-pass for the topography mapping, in which the AFM is operated in standard tapping mode.¹⁶ It should be noticed that other modes for topography mapping, such as the peakforce tapping mode,¹⁷ can also be used in the first-pass. The scanning TENG mode is operated in the second-pass [red block diagrams in Fig. 1(c)], in which the tip is raised above the sample

surface with a certain lift height (h), and scans the surface along the topographic profile. Meanwhile, the tip is mechanically excited by the tapping piezo to vibrate at resonant frequency (ω) with a certain tapping amplitude (A_0). And the AC signal between the conductive tip and the bottom electrode is collected by using a current application. Further, the AC signal is fed into a lock-in amplifier (lock-in 2), and the reference frequency of lock-in 2 is set to be ω , so that the amplitude of ω frequency component current can be extracted from the AC signal. It needs to be clarified that the AC signal needs to be converted into a voltage signal before it is fed into a lock-in amplifier. And there is a signal attenuation in the coupling between the current application and the lock-in amplifier. But anyway, the amplitude output of the lock-in amplifier is linear in relation to the amplitude of the ω frequency component of AC between the tip and the bottom electrode, with a certain linear coefficient (α). It means that if the amplitude output of the lock-in amplifier is A_c , the amplitude of the first harmonic (ω frequency component) of the induced AC should be αA_c . According to Eq. (5), the surface charge density (σ) can be expressed as follows:

$$\sigma = \frac{\varepsilon\varepsilon_0 V}{d} - \frac{\alpha\varepsilon A_0 A_c}{2\omega S d \left(\frac{d + \varepsilon h}{\sqrt{(d + \varepsilon h)^2 - (\varepsilon A_0)^2}} - 1 \right)}. \quad (6)$$

In Eq. (6), several parameters need to be measured, among which the effective area of the tip (S) is difficult to be measured accurately. In order to ensure the accuracy of the scanning TENG, we propose a self-calibration method here. We let the constant

$$k = \frac{\alpha\varepsilon A_0}{2\omega S d \left(\frac{d + \varepsilon h}{\sqrt{(d + \varepsilon h)^2 - (\varepsilon A_0)^2}} - 1 \right)}. \quad (7)$$

Then, Eq. (6) can be expressed as

$$A_c = \frac{\varepsilon\varepsilon_0 V}{kd} - \frac{\sigma}{k}, \quad (8)$$

and

$$\sigma = -kA_c + \frac{\varepsilon\varepsilon_0 V}{d}. \quad (9)$$

According to Eq. (8), the constant k can be calibrated by applying a different bias between the tip and the bottom electrode. The amplitude output of the scanning TENG (A_c) should vary linearly with the applied bias, and the slope represents the parameter $\left(\frac{\varepsilon\varepsilon_0}{kd}\right)$, in which ε and ε_0 depend on the dielectric materials and the thickness of the dielectric film d can be measured accurately. After the constant k is calibrated, the surface charge density can be calculated by using Eq. (9).

We established the scanning TENG mode based on a commercial AFM equipment. A pure Pt tip (its resonant frequency was measured to be 66 kHz) was used in the experiments, and a Kapton thin film (with 100 nm thickness) deposited on heavily doped silicon wafer was used as the sample, which is one of the most commonly used materials in TENG. (More details about the experiments are shown in supplementary material note 2.) We set the A_0 and h to be 100 nm in the

scanning TENG experiments, and the mapping of the amplitude output of scanning TENG with different bias applied on the tip is shown in Fig. 2(a). It is found that amplitude output of the scanning TENG varied linearly with the applied bias between the tip and the bottom electrode, as shown in Fig. 2(b). By fitting the relationship between the applied bias and the amplitude output, the parameter $\left(\frac{\varepsilon\varepsilon_0}{kd}\right)$ is calculated to be -0.84×10^{-3} , and the constant k is further calculated to be -0.36 F/m^2 . We notice that the amplitude output of the scanning TENG reached 24.25 mV, though the applied tip bias is 0. This is the background signal in the system, and its phase is opposite to that of the first harmonic of the induced current, so that the constant k is negative. The background signal does not affect the accuracy of the calibration, since that only the slope of the line is concerned.

After the calibration, scanning TENG was used to measure the charge density on the dielectric surface. Adjacent positive and negative charges were first injected into the Kapton sample surface by rubbing it with a biased pure Pt tip (+10 V for positive charges and -10 V for negative charges) in contact mode with $10 \mu\text{m}$ scan size. Then, the equipment was operated in scanning TENG mode to map the induced current amplitude on the charged region and the scan size was $20 \mu\text{m}$ and scan rate was 0.5 Hz. Figure 3(a) shows the mapping of the amplitude output, in which the background signal is subtracted. It can be seen that positive charges on the Kapton surface increased the amplitude output of the scanning TENG (left side) and the negative charges decreased the amplitude output (right side). Figure 3(b) gives the profile of the cross section in Fig. 3(a), in which the change of amplitude output (ΔA_c) induced by the surface charges reached about $\pm 1.6 \text{ mV}$.

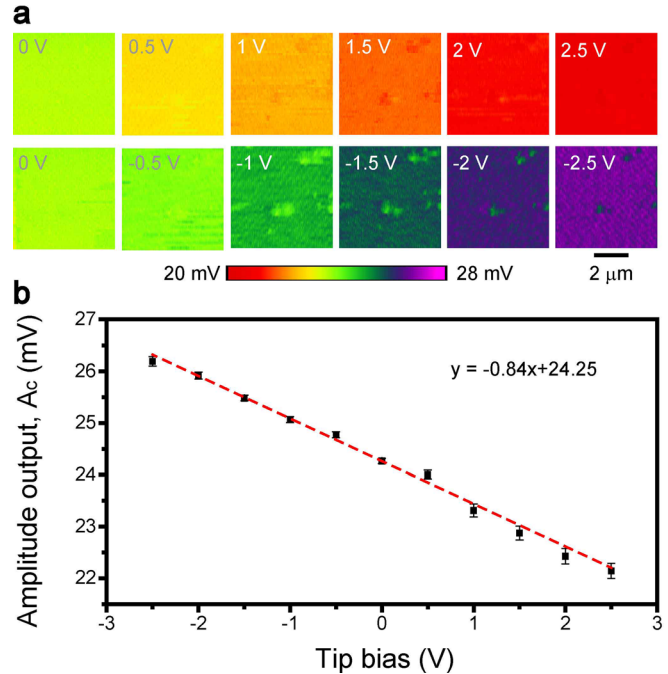


FIG. 2. Bias effect on the amplitude output of scanning TENG mode. (a) The mapping of the amplitude output on the Kapton surface in scanning TENG mode with different applied bias on the tip. (b) The linear relationship between the amplitude output and the tip bias.

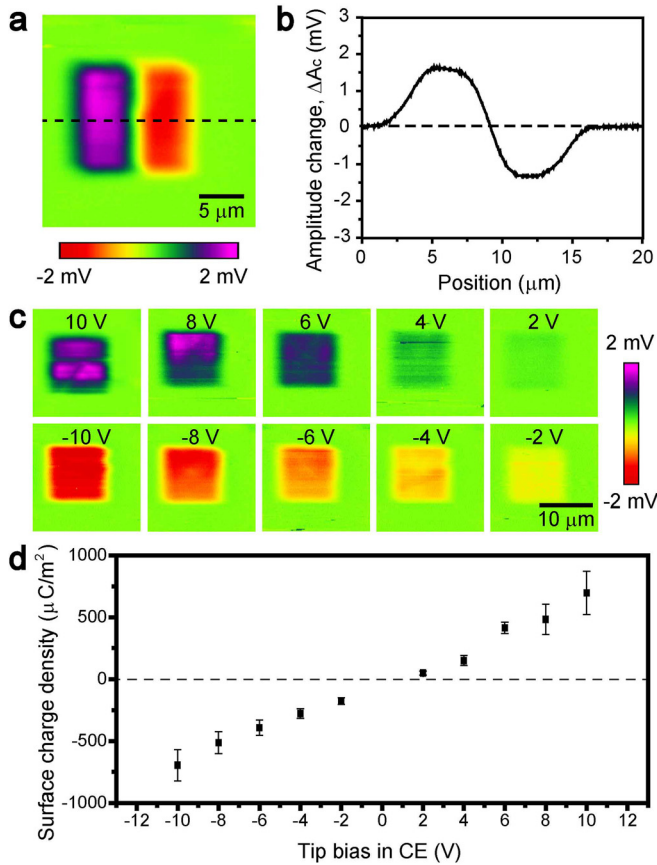


FIG. 3. Measurement of surface charge density by using scanning TENG mode. (a) The amplitude mapping in scanning TENG mode, which is induced by the positive and negative charges on the Kapton surface. (b) The profile of the mapping in (a). (c) The scanning TENG mappings of the Kapton surfaces, on which the charges are injected by a conductive tip with different biases various from -10 V to $+10\text{ V}$. (d) The relation between the tip bias in contact-electrification and the transferred charge density on the Kapton surface, which is measured by using the scanning TENG.

According to Eq. (9), the contribution of the transferred surface charge density on the amplitude output change (ΔA_c) can be expressed as follows:

$$\Delta\sigma = -k\Delta A_c. \quad (10)$$

In Eq. (10), both the constant k and the amplitude change (ΔA_c) are known, the transferred surface charge density on the Kapton surface, which is generated by rubbing with the biased Pt tip, is calculated to be about $\pm 576\ \mu\text{C}/\text{m}^2$.

The scanning TENG was further used to measure the transferred charge density on the Kapton surfaces, which were rubbed by a pure Pt tip with different tip biases various from -10 V to $+10\text{ V}$. In the scanning TENG mappings as shown in Fig. 3(c), it is shown that a higher tip bias during rubbing will induce a larger current amplitude output change. Based on Eq. (10), the relation between the tip bias and the transferred surface charge density between the tip and Kapton sample is obtained as shown in Fig. 3(d). It is obvious that a higher tip

bias induced a higher surface charge density, which is consistent with previous studies. These results suggest that scanning TENG can be used to measure the surface charge density of a dielectric material.

In order to further check the theoretical model for scanning TENG, the effect of the tip lift height (h) and tapping amplitude (A_0) on the scanning TENG output (ΔA_c) was investigated. The negative charges were first injected into Kapton surface by rubbing with a -10 V biased Pt tip, and then, the scanning TENG mode was used to scan the charged surface with different parameter settings. Figure 4(a) shows the effect of lift height on the mapping of the scanning TENG, when the tapping amplitude was kept equal to the lift height. It is found that the change of induced current amplitude remained almost unchanged when the tapping amplitude equal to the lift height, though they varied from 20 nm to 180 nm. If the tip tapping amplitude is kept at 100 nm, and the lift height vary from 100 nm to 200 nm, the change of the induced current amplitude will decrease, as shown in Fig. 4(b). This is because that the electrostatic interaction between the tip and the surface charges decreases when the distance between the tip and dielectric surface increases. We put the experiment parameters (h and A_0) into Eq. (7), and it is found that the change of constant k is limited if the tapping amplitude equal to the lift height. If the tip tapping amplitude is kept at a constant value, the constant k will increase in value with the increasing of the lift height, resulting in a decrease in

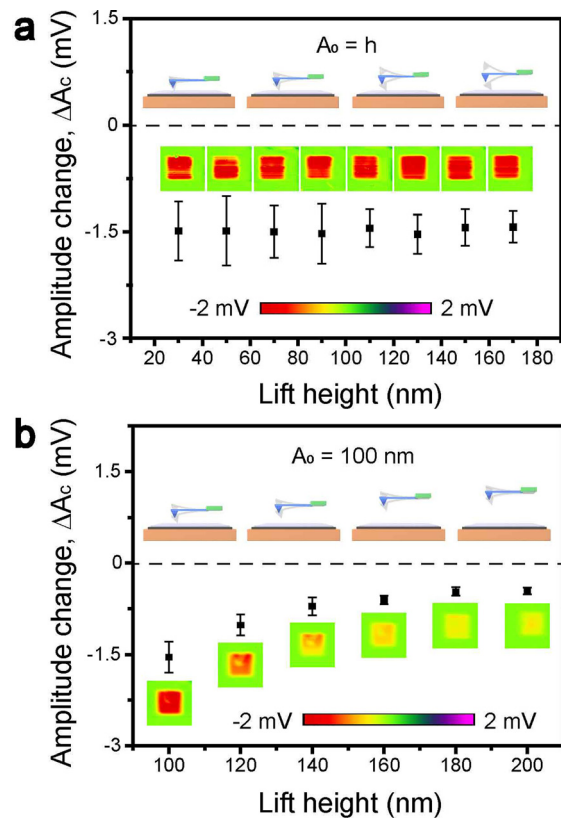


FIG. 4. The effect of the tip lift height on the scanning TENG measurements, (a) when the tapping amplitude is equal to the light height and (b) when the tapping amplitude remain constant.

the induced current amplitude. It means that the experiment data are consistent with the theoretical model for scanning TENG.

As a comparison, adjacent positive and negative charges on Kapton surface, which was generated by rubbing with a biased conductive tip (+10 V and −10 V), was also measured by using KPFM. In the KPFM mode, a Pt coated tip was used, and the mapping of the surface potential is shown in [supplementary material Fig. 1\(a\)](#), in which the background signal is also subtracted. The surface potential of the Kapton sample became more positive due to the positive charges on the surface, and it became more negative due to the negative charges on the surface, as expected. The profile in [supplementary material Fig. 1\(b\)](#) shows that the change of surface potential induced by the surface charges reached about ± 2.2 V. According to Eq. (11),^{18,19} the surface charge density measured by KPFM mode is calculated to be $\pm 584 \mu\text{C}/\text{m}^2$, which is very close to the value measured by using scanning TENG mode, as shown in [Figs. 3\(a\) and 3\(b\)](#). The difference between them is less than 1.4%.

$$\Delta\sigma = \frac{\epsilon\epsilon_0\Delta V}{d}. \quad (11)$$

It turns out that both KPFM and scanning TENG can be used to measure the surface charge density, but they work on different principles. Comparing to KPFM mode, AC bias or DC bias between tip and sample is not required in scanning TENG mode, thus avoiding some potential effects of the biases on the sample. More importantly, the scanning TENG works in exactly the same way as the contact-separation mode TENG. The output of the scanning TENG is the amplitude of the induced AC, which is highly concerned in the studies about the energy harvesting by using TENG. Therefore, the scanning TENG can not only be used to measure the transferred charge density in contact-electrification, but also provides a method for analyzing the current output of the TENG. Based on the scanning TENG, the structure of the TENG, such as the thickness of the dielectric layer, distance between the electrode and the dielectric surface, vibration amplitude of the electrode, can be optimized. Also, triboelectric properties of the dielectric materials for TENG can be characterized at nanoscale.

In summary, inspired by the contact-separation mode TENG, the scanning TENG was invented to measure the charge density on dielectric surfaces at nanoscale. The AC output of the scanning TENG was analyzed by using Fourier transform. The calculations show that the amplitude of the first harmonic of the induced AC between the tip and the bottom electrode is linearly related to the surface charge density of the dielectric sample. Further, the scanning TENG was established based on a commercial AFM equipment. The effect of difference parameters on the scanning TENG measurement was discussed. Comparing to the KPFM mode, there is no AC or DC bias between the conductive tip and the bottom electrode in the scanning

TENG mode, and the scanning TENG has more implications in the studies about the TENG.

See the [supplementary material](#) for the results of the KPFM measurement and the details of the calculations.

The authors thank Dr. Jiajia Shao (BINN) and Linliang Zhang (Beijing Jiaotong University) for checking the calculations and thank Dr. Yang Liu (Bruker) and Weiqi Wang (SKLT, Tsinghua University) for their help in the AFM experiments. Research was supported by the National Key R & D Project from Minister of Science and Technology (No. 2016YFA0202704), National Natural Science Foundation of China (Grant No. 52005044), Beijing Municipal Science & Technology Commission (Nos. Z171100002017017 and Y3993113DF). The patent of the techniques introduced in this work has been applied.

DATA AVAILABILITY

The data that support the findings of this study are available from the corresponding author upon reasonable request.

REFERENCES

- ¹T. Choi, Y. Horibe, H. T. Yi, Y. J. Choi, W. Wu, and S. Cheong, *Nat. Mater.* **9**, 253 (2010).
- ²M. Dawber, C. Lichtensteiger, M. Cantoni, M. Veithen, P. Ghosez, K. Johnston, K. Rabe, and J. Triscone, *Phys. Rev. Lett.* **95**, 177601 (2005).
- ³M. Nonnenmacher, M. Oboyle, and H. Wickramasinghe, *Appl. Phys. Lett.* **58**, 2921 (1991).
- ⁴C. Lei, A. Das, M. Elliott, and J. Macdonald, *Nanotechnology* **15**, 627 (2004).
- ⁵R. Cannara, M. Eglin, and R. Carpick, *Rev. Sci. Instrum.* **77**, 053701 (2006).
- ⁶D. rugatr, H. Mamin, P. Guethner, S. Lambert, J. Stern, I. Mcfadyen, and T. Yogi, *J. Appl. Phys.* **68**, 1169 (1990).
- ⁷G. Yeroslavsky, O. Girshevitz, J. Foster-Frey, D. Donovan, and S. Rahimipour, *Langmuir* **31**, 1064 (2015).
- ⁸F. Fan, Z. Tian, and Z. L. Wang, *Nano Energy* **1**, 328 (2012).
- ⁹M. Muthu, R. Pandey, X. Wang, A. Chandrasekhar, I. Palani, and V. Singh, *Nano Energy* **78**, 105205 (2020).
- ¹⁰A. Mathew, A. Chandrasekhar, and S. Vivekanandan, *Nano Energy* **80**, 105566 (2021).
- ¹¹C. Sukumaran, V. Vivekananthan, V. Mohan, Z. Alex, A. Chandrasekhar, and S. Kim, *Appl. Mater. Today* **19**, 100625 (2020).
- ¹²W. Melitz, J. Shen, A. Kummel, and S. Lee, *Surf. Sci. Rep.* **66**, 1 (2011).
- ¹³R. Cheedarala, A. Parvez, and K. Ahn, *Nano Energy* **53**, 362 (2018).
- ¹⁴Q. Guo and C. Liu, *Nano Energy* **76**, 104969 (2020).
- ¹⁵S. Niu, S. Wang, L. Lin, Y. Liu, Y. Zhou, Y. Hu, and Z. L. Wang, *Energy Environ. Sci.* **6**, 3576 (2013).
- ¹⁶R. Stark, T. Drobek, and W. Heckl, *Appl. Phys. Lett.* **74**, 3296 (1999).
- ¹⁷B. Zhao, Y. Song, S. Wang, B. Dai, L. Zhang, Y. Dong, J. Lu, and J. Hu, *Soft Matter* **9**, 8837 (2013).
- ¹⁸S. Lin, L. Xu, A. Wang, and Z. L. Wang, *Nat. Commun.* **11**, 399 (2020).
- ¹⁹Y. Zhou, Y. Liu, G. Zhu, Z. Lin, C. Pan, Q. Jiang, and Z. L. Wang, *Nano Lett.* **13**, 2771 (2013).